Low-Dispersive Leaky-Wave Antennas for mmWave Point-to-Point High-Throughput Communications

Low-Dispersive Leaky-Wave Antennas for mmWave Point-to-Point High-Throughput Communications

Oskar Zetterstrom, *Student Member, IEEE*, Elena Pucci, Pablo Padilla, Lei Wang, *Senior Member, IEEE*, and Oscar Quevedo-Teruel, *Senior Member, IEEE*

(Invited Paper)

***Abstract*— In this article, we present two efficient leaky-wave antennas (LWAs) with stable radiation pattern, operating at 60 GHz. Both antennas exhibit attractive properties such as significantly reduced beam-squint, low loss, low sidelobes, high directivity, and simple manufacturing. The beam-squint of conventional LWAs is reduced by refracting the leaked waves in a dispersive lens and the low sidelobe levels are achieved by tapering the leakage rate along the aperture. Since the antennas are implemented in groove gap waveguide technology, the losses are low. The two antennas are different in terms of their asymmetric/symmetric leakage tapering with respect to the broadside direction. Both designs are optimized for low sidelobes, but since symmetry is enforced in one, the resulting performance in terms of sidelobes is suboptimal. However, in the symmetric design, multiple stable beams can be obtained, simultaneously or independently. Twenty percent bandwidth is obtained with less than ±0.5° beam-squint. In this frequency range, the gain is stable at 17 and 15 dBi for the asymmetric and symmetric designs, respectively. The designs are intended for point-to-point links in mmWave communication networks where low losses, directive beams, and low sidelobes are expected to be key features.**

***Index Terms*— 5G, gap waveguide, leaky-wave antenna (LWA), mmWave, reduced beam-squint.**

I. Introduction

GAP waveguide technology provides attractive characteristics for high-frequency communications, for instance, relatively low manufacturing cost for low loss guiding structures [1], [2] and straightforward implementation of microwave devices [3]–[5]. However, the design of directive antennas implemented in gap waveguide technology is still a challenge. The challenge arises due to the high operating frequency in which gap waveguides are advantageous compared to conventional technologies. The high frequency translates into a need for fully metallic structures and small manufacturing details. Due to the intrinsic layered nature of gap waveguides, 2-D array solutions, in which multiple layers are used to construct the feeding network and radiating elements, were initially proposed as a means of achieving high gain [6], [7]. While resulting in relatively simple and reliable manufacturing, the complex and cumbersome design of the feeding network, which is obstructed by the space required for the electromagnetic band gap (EBG) structure at the lateral sides of the waveguides, results in large interelement distance in the array which produces high sidelobes.

Recently, gap waveguide leaky-wave antennas (LWAs) were proposed [8], [9]. The main benefit of LWAs, especially in high frequency applications, is their ability of producing directive radiation with a very simple feeding structure, contrary to the previously proposed 2-D arrays. Moreover, it has been shown that an increased control of the aperture fields can be exerted in this type of antennas [10]. This additional control can be used to produce desired far-field properties, such as low sidelobes or broad beamwidth. However, the inherent dispersion of the feeding waveguide causes the radiated beam to scan with frequency [11]. While sometimes desired (for instance, in radar and imaging applications), this beam scanning limits the applicability of LWAs in many scenarios, e.g., high-frequency point-to-point communications. Moreover, as directivity increases, the beamwidth decreases, and the scanning becomes more detrimental, which further limits the effective bandwidth of the antenna.

The beam scanning of LWAs is well known and several techniques to reduce or cancel it completely have been proposed [12]–[23]. The reported techniques can be divided into five categories. First, in [12], it is demonstrated that a reduced scanning in the radiation pattern can be obtained if the radiating aperture is divided into several subapertures, each responsible for the radiation in a narrow frequency range. However, since the aperture is divided, this results in reduced directivity. The same concept is used in [13] and [14], resulting in similar deterioration. Second, in [15], a technique for reduced beam-squint, which does not suffer from reduced directivity, is proposed. The authors demonstrated that a wideband squint-free radiation of energy can be obtained if a nondispersive guided wave is traveling at the interface between two medias. A "leaky-lens" can be designed by printing a slot on the back of a dielectric and the guided wave in the slot is leaked into the dielectric. However, since the leakage only occurs in the pres-

Manuscript received April 18, 2019; revised August 31, 2019; accepted September 2, 2019. Date of publication October 11, 2019; date of current version March 3, 2020. This work was supported in part by the Vinnova Project High-5 through the Strategic Programme on Smart Electronic Systems under Grant 2018-01522 and in part by the Stiftelsen ÅForsk Project H-Materials under Grant 18-302. *(Corresponding author: Oskar Zetterstrom.)*

O. Zetterstrom and O. Quevedo-Teruel are with the Division of Electromagnetic Engineering, KTH Royal Institute of Technology, 100 44 Stockholm, Sweden (e-mail: oskdah@kth.se).

E. Pucci is with Systems and Technology, Ericsson AB, 164 80 Stockholm, Sweden.

P. Padilla is with the Departamento de Teoría de la Señal, Telemática y Comunicaciones, Universidad de Granada, 180 71 Granada, Spain.

L. Wang is with the Institut für Theoretische Elektrotechnik, Hamburg University of Technology, 21079 Hamburg, Germany.

Color versions of one or more of the figures in this article are available online at http://ieeexplore.ieee.org.

Digital Object Identifier 10.1109/TAP.2019.2943437

ence of a dielectric, this technique is inherently lossy, especially at high frequencies. Third, in [16] and [17], the beam-squint is reduced by coupling the leaked energy through one or multiple cavities, placed in-front of the radiating aperture. While significantly reducing the beam-squint, the resulting radiation pattern is distorted and high sidelobes appear. Fourth, in [18], non-Foster circuits which can be used to eliminate the beam-squint in a finite frequency range are proposed. This method is quite general and can be applied to arrays as well as LWAs, but active components and biasing are required, resulting in decreased overall efficiency of the system. Finally, several attempts to reduce the beam scanning using metamaterials/metasurfaces have been reported. In [19], a 1-D nonreciprocal transmission line was proposed, in which the beam-squint reduction is achieved through the radiation of two waves traveling in opposite directions on the line, with different phase velocities (due to non-reciprocity). However, since nonreciprocal materials are required, the realization of such a system is difficult. Similarly, in [20], squint-free radiation is achieved by combining two leaky waves traveling in opposite directions along a 1-D transmission line. However, while the main beam is squint free, the radiation pattern changes over the operation bandwidth. Mehdipour *et al.* [21] proposed a method of reducing the dispersion of an LWA by refracting the radiated fields through a Huygens' metasurface. The dispersion of the metasurface must be such that waves of different frequencies, impinging from different directions, are refracted into one direction at the other side of the metasurface. Although it is theorized that a complete squint-free radiation is possible, the beam-squint is only reduced by a factor of 2 in [21]. In [22] and [23], a similar concept is applied, but instead of a Huygens metasurface, a dispersive lens is placed in front of the radiating aperture. The lenses are implemented using metasurfaces. Again, the dispersion of the lens must be such that the refracted fields in the lens are focused into one direction. In these works, an almost full cancellation of the beam squint is achieved.

In this article, we apply the same concept as in [22] and [23] in the design of two directive antennas at mmWave frequencies. Similar to [23], the antennas are implemented in groove gap waveguide technology, resulting in low losses. The novelty of this work is threefold. First, we demonstrate how reduced sidelobes can be obtained simultaneously to reduced beam-squint. Second, we demonstrate how the technique in [22] and [23] can be used to design directive multibeam antenna systems. Third, we have significantly increased the operational frequency, compared to [23], which implies technological and manufacturing challenges. The intended application for the proposed systems is point-to-point communications for future mobile communication networks (5G and beyond), where high directivity, low sidelobes, low losses, and multibeam capabilities are desired [24]. This article is outlined as follows: in Section II, the operational principle of the antenna is explained. In Section III, two design examples are detailed. In Section IV, the design examples are experimentally verified, and finally, in Section V, conclusions are drawn.

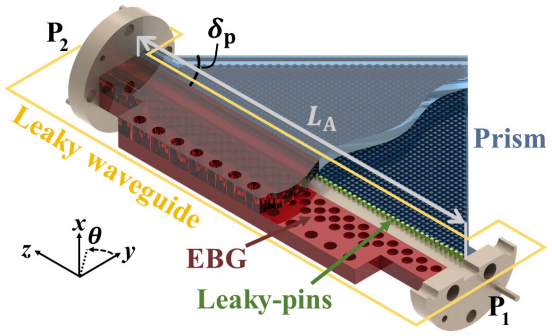

Fig. 1. Illustration of the proposed antenna. There are two main parts: leaky-wave gap waveguide (yellow) and dispersive prism (blue).

II. Design Principles of Low-Dispersive LWAs With Reduced Sidelobe Levels

An illustration of the design used for both antennas is presented in Fig. 1, and it consists of two main components: the leaky waveguide (in yellow) and the dispersive prism (in blue). The design procedure is similar to the one in [22] and [23] but, for completeness, the important steps are repeated below. The additional techniques employed in order to improve the radiation performance are indicated in the following as well. First, the technique used for the reduction of sidelobes is discussed (Section II-A). Second, the reduction of the beam-squint is presented (Section II-B).

A. LWA With Reduced Sidelobe Levels

In point-to-point communications, a low sidelobe level (SLL) is desired in order to reduce interference. Such characteristics in the far-field pattern can be obtained by illuminating the aperture with a sinusoidal distribution [11]. The relationship between the magnitude of the complex aperture distribution, $A(z)$, and the imaginary part (α) of the complex propagation constant in the leaky guiding structure ($\beta - j\alpha$) is given by [25]

$$|A(z)| = \sqrt{\alpha(z)}\mathrm{e}^{-\int_0^z \alpha(t)dt} \tag{1}$$

where z is the position along the aperture. By solving (1) for α/k_0 (as is done in [26]) under the assumption that a sinusoidal aperture distribution (i.e $|A(z)| = \sin(\pi z/L_\mathrm{A})$) is desired, we obtain

$$\alpha/k_0(z) = \frac{\frac{1}{2k_0}|\sin\left(\frac{\pi z}{L_\mathrm{A}}\right)|^2}{\frac{1}{\eta}\int_0^{L_\mathrm{A}}|\sin\left(\frac{\pi z}{L_\mathrm{A}}\right)|^2 d\xi - \int_0^z |\sin\left(\frac{\pi z}{L_\mathrm{A}}\right)|^2 d\xi} \tag{2}$$

where L_A is the length of the leaking aperture and k_0 is the free-space propagation constant. In order to efficiently radiate over some bandwidth, the radiation efficiency η is set to 90%–95%. Additionally, the real part of the propagation constant, β, must remain fixed throughout the aperture in order to radiate coherently from every section of the structure. The desired aperture distribution for reduced sidelobes and the corresponding $\alpha/k_0(z)$- and β-profiles are illustrated in Fig. 2.

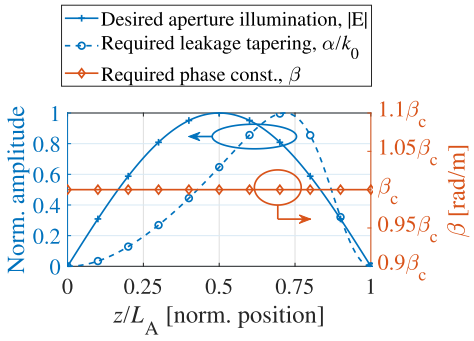

Fig. 2. Desired E-field aperture distribution, α/k_0- and β profiles for reduced sidelobes.

The tapered leakage can be obtained by gradually changing the dimensions of the waveguiding structure along the aperture. Therefore, this leakage is structure independent and low-sidelobe LWAs can be implemented in different technologies, e.g., gap waveguide [10], substrate integrated waveguide (SIW) [27], and microstrip [28]. Far-fields with other properties, for instance, near-field focusing, control of the radiation nulls, and broad beamwidth, can be obtained if other leakage profiles are employed [25], [27].

B. LWA With Reduced Beam-Squint

In this article, the beam-squint of conventional LWAs is reduced by coupling the leaked energy through a dispersive prism-lens. A similar approach was followed in [22] and [23]. Prisms are structures that, for impinging waves of different wavelengths, refract the light in different directions. This spatial division of the spectral components of the impinging light occurs due to the frequency-dependent refractive index in the prism. Prisms can operate in one of two modes. In the first operational mode, prisms split the spectral components of white light (i.e., light with a wide range of wavelengths) incident from a single direction into several directions depending on frequency. In the second operational mode, prisms gather a colored light (i.e., light concentrated in a narrow range of wavelengths) impinging from different directions into white light traveling in one direction. In this article, the employed prism is operated in the second mode. Although prisms exist in a variety of shapes, we will focus our analysis to triangular prisms. The operating principle of the antenna is illustrated in Fig. 3.

In conventional LWAs, the beam-squint arises from the dispersive nature of the waveguide mode. The direction of maximum radiation is given by

$$\sin[\theta_{\rm l}(f)] = \frac{\beta_{\rm l}}{k_0} = n_{\rm eff,leaky}(f) \tag{3}$$

where $\beta_{\rm l}$ and k_0 are the propagation constants in the leaky waveguide and free-space, respectively. The scanning of the leaky-wave radiation is illustrated in Fig. 3 (left). There, the radiation from the leaky structure is spatially divided into its spectral components, and in conventional LWAs, the direction of maximum radiation scans from broadside to endfire

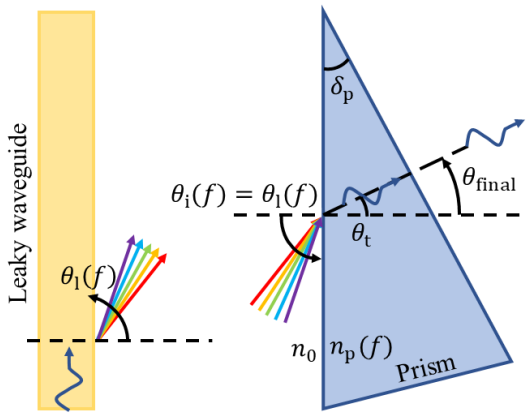

Fig. 3. Illustration of working principle for reduced beam-squint. For a range of frequencies, the dispersive radiation from the leaky waveguide is refracted into a single direction with a dispersive prism. The prism inclination, $\delta_{\rm p}$, is chosen so there is no refraction at the edge of the prism and hence, $\theta_{\rm t} = \theta_{\rm final} = \delta_{\rm p}$.

when the frequency increases. By placing a prism in front of the leaky aperture, this scanning can be canceled.

The required characteristics of the prism can be found through the Snell's law, which describes the refraction through an interface

$$n_1 \sin(\theta_{\rm i}) = n_2 \sin(\theta_{\rm t}) \tag{4}$$

where n_1 and n_2 are the refractive indices on each side of the interface and $\theta_{\rm i}$ and $\theta_{\rm t}$ are the impinging and refracted angles, respectively. n_1 and/or n_2 may be, in general, frequency dependent. For this analysis, the first medium is assumed to be air ($n_1 = n_0 = 1$). The second medium corresponds to the prism, which we will assume is frequency dependent ($n_2 = n_{\rm p}(f)$). The impinging angle is given by the direction of maximum radiation of the leaky waveguide, i.e. $\theta_{\rm i} = \theta_{\rm l}(f)$. By substituting these assumptions in (4), we obtain

$$\sin(\theta_{\rm i}) = n_{\rm p}(f)\sin(\theta_{\rm t}) \Rightarrow \theta_{\rm t} = \arcsin\left(\frac{\sin[\theta_{\rm l}(f)]}{n_{\rm p}(f)}\right). \tag{5}$$

It is clear that, since the impinging angle varies with frequency, the light of different wavelengths is refracted into one single direction, given that the refractive index in the prism neutralizes this variation. For conventional LWAs, $\sin[\theta_{\rm l}(f)]$ increases with frequency, and hence, in order to reduce the beam-squint, the refractive index of the prism must also increase with frequency. Furthermore, in order to avoid to again spatially divide the spectral components of the light at the second interface of the prism, the prism inclination, $\delta_{\rm p}$, is chosen so that $\theta_{\rm t}$ (i.e., the refracted angle) is normal to the second interface. In conclusion, if a prism can be devised with the correct frequency behavior of the refractive index $n_{\rm p}(f)$, a non-squinting LWA can be realized. Noteworthy is that, throughout this analysis, no assumption on the type of guiding structure has been made, and thus, this technique is structure independent, contrary to, for instance, the technique used in [15]. In fact, it has been used successfully for both SIW LWAs [22] and groove-type gap waveguide LWAs in the X-band [23].

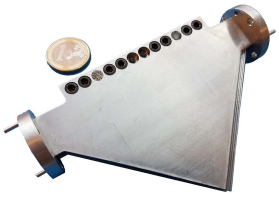

(a)

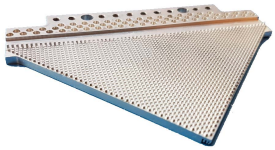

(b)

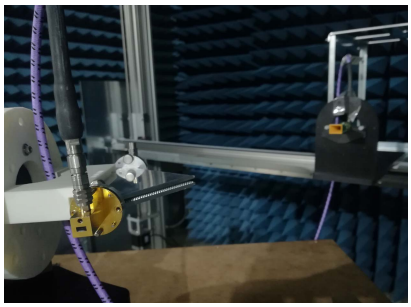

(c)

Fig. 4. Realized prototype of the asymmetric design. (a) Closed, (b) bottom piece, and (c) far-field measurement setup. A 1€ coin has been included for reference.

(a)

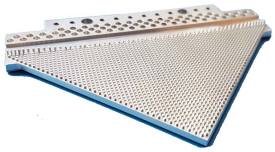

(b)

(c)

Fig. 5. Realized prototype of the symmetric design. (a) Closed, (b) bottom piece, and (c) far-field measurement setup. A 1€ coin has been included for reference.

III. Design Examples

Two LWAs are designed using the procedures outlined in Section II. In this article, denoted as *asymmetric* and *symmetric*. The two designs differ in the implemented leakage profile. The asymmetric LWA is designed to have the lowest possible sidelobes with a single fixed beam. The symmetric LWA, on the other hand, is designed to have low sidelobes with a symmetric leakage tapering with respect to the broadside direction. Thus, the symmetric design enables beam-switching by feeding from either end of the leaky waveguide (P_1 and P_2 in Fig. 1). Both antennas have a center frequency of 60 GHz. The realized prototypes are shown in Figs. 4 and 5 for the asymmetric and symmetric designs, respectively.

A. Leaky Groove Gap Waveguide

Since the target is mmWave communications, the antennas are implemented in groove gap waveguide technology [1], [2], [29]–[31]. Due to the high operating frequency, the EBG-structure in the groove gap waveguide, opposite to the prisms as showed in Fig. 1, consists of a 2-D periodic repetition of glide-symmetric holes [32], [33]. A glide-symmetric structure is, contrary to purely periodic structures, composed of two subunit cells. The geometrical operation, applied to the subunit cells in a glide-symmetric structure, consists of a translation of $p/2$, where p is the translational period of the full unit cell, and a mirroring [34]. In the case of Cartesian glide symmetry, which is the symmetry employed here, the mirroring is done with respect to a plane. Glide-symmetric metasurfaces have shown attractive properties such as very low-frequency dispersion [35], [36], increased equivalent refractive index [37], [38] (extremely large indices reported [39]), and huge stop bands at selected frequencies [32], [33]. Moreover, glide-symmetric holey EBG structures have larger unit cells, are less expensive to manufacture, and are more robust, compared to a bed-of-nails structure [5], [32], [33]. These interesting properties of glide symmetry have been extensively studied over the last few years and several numerical methods have been reported which give valuable physical insight on this technology [40]–[43].

Due to their larger physical dimensions, glide-symmetric EBG structures are especially attractive at high frequencies (submillimeter wavelength). As a matter of fact, gap waveguides employing a glide-symmetric holey EBG structure operating up to 170 GHz have been presented [44]. Additionally, by decreasing the undesired gap between the two parallel plates, the width of the stopband increases while remaining centered at the same frequency, which further simplifies manufacturing and assembly [32], [45]. In [33], it was shown that a single row of a glide-symmetric holey EBG is enough to suppress the leakage in a straight waveguide. The unit cell of the EBG-structure used in the gap waveguide is shown in Fig. 6(a) (red), together with the dispersion diagram (red curve). The dimensions used for the simulation are $r_h = 1.3$ mm, $d_h = 1.1$ mm, $g = 0.05$ mm, and $p_{EBG} = 3.2$ mm. A full stopband is obtained, ranging from 45 to 80 GHz. In Fig. 6(a), only the first part of the Brillouin diagram is presented. However, the full stopband (i.e., for the full irreducible Brillouin diagram) is marked by the red area.

In [9], it was shown that a groove-type gap waveguide can be transformed into a leaky-wave antenna by removing the EBG-structure on one of the sides of the groove. Furthermore, if the removed EBG-structure is instead replaced with a longitudinal structure (with respect to the waveguiding direction), the leakage can be controlled along the aperture, and the profile necessary for reduced sidelobes can be obtained. In this work, similar to the designs presented in [9], [10], and [23], periodically repeated square pins, placed along the groove,

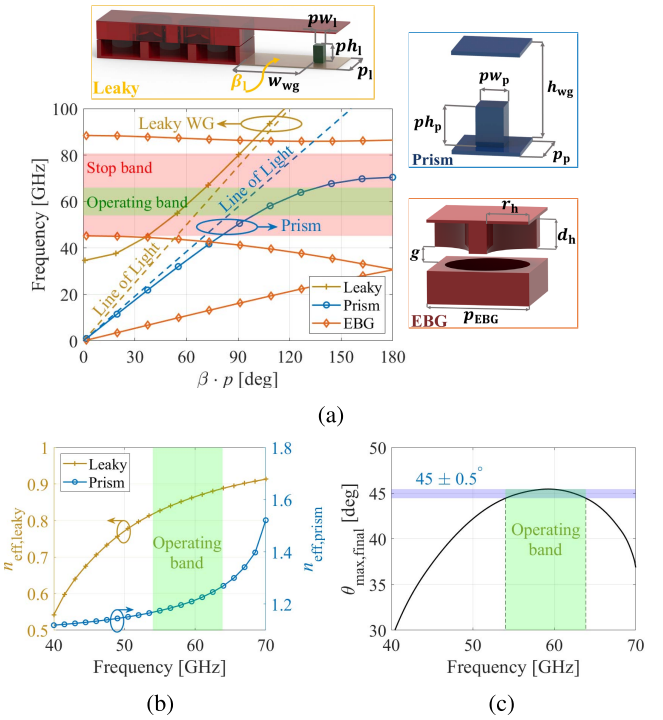

Fig. 6. Simulation results assuming infinitely periodic structures. (a) Dispersion curves for the different components with the unit cells in the insets. (b) Effective refractive index for the leaky mode and the prism. (c) Calculated final (leaky mode and prism combined) direction of maximum radiation. Dimensions: $h_{\mathrm{wg}} = 2.39$ mm, $pw_{\mathrm{l}} = 0.7$ mm, $r_{\mathrm{h}} = 1.3$ mm, $d_{\mathrm{h}} = 1.1$ mm, $g = 0.05$ mm, $p_{\mathrm{EBG}} = 3.2$ mm, $ph_{\mathrm{p}} = 0.7$ mm, $pw_{\mathrm{p}} = 0.7$ mm, and $p_{\mathrm{p}} = 1.3$ mm. To obtain these results, $p_{\mathrm{l}} = 1.5$ mm, $ph_{\mathrm{l}} = 1.5$ mm, and $w_{\mathrm{wg}} = 4.8$ mm have been used. However, these three dimensions are tapered throughout the structure. Their values along the structure are given in Figs. 7 and 8 for the asymmetric and symmetric designs.

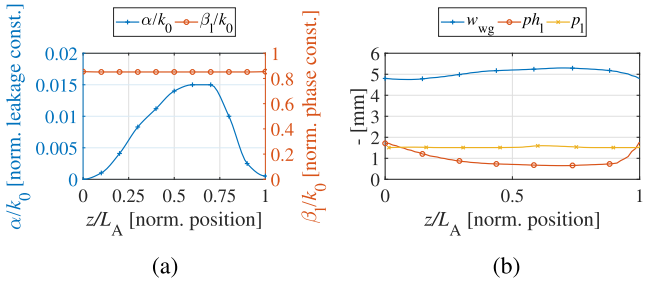

Fig. 7. Design profiles in the asymmetric design. (a) Targeted leakage profile and (b) waveguide parameter profiles to synthesize the leakage profile in (a). The mapping is done at 60 GHz.

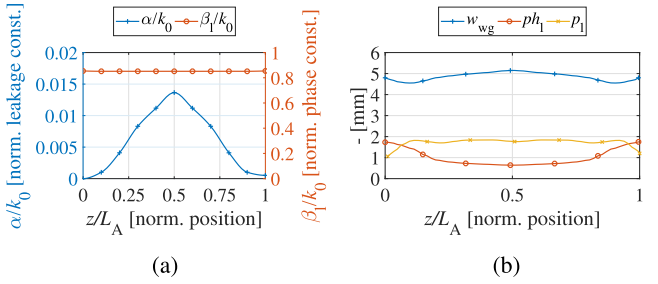

Fig. 8. Design profiles in the symmetric design. (a) Targeted leakage profile and (b) waveguide parameter profiles to synthesize the leakage profile in (a). The mapping is done at 60 GHz and the leakage is symmetric in the z-direction with respect to the center of the leaky waveguide.

are employed to control the leakage (in order to reduce the sidelobes). These pins are here denoted *leaky pins* and are marked with green in Figs. 1 and 6(a). The leakage rate is mainly determined by the height, ph_{l}, and periodicity, p_{l}, of the leaky pins. The control of propagation constant of the waveguide mode, β_{l}, is mainly exerted through the width of the leaky waveguide, w_{wg}. Since the geometry of the waveguide is varied, the dispersion diagram changes along the structure, but for reference, the dispersion diagram for one sample of the leaky mode, β_{l}, is presented in Fig. 6(a) (yellow curve). For this sample, the dimensions are $h_{\mathrm{wg}} = 2.39$ mm, $pw_{\mathrm{l}} = 0.7$ mm, $p_{\mathrm{l}} = 1.5$ mm, $ph_{\mathrm{l}} = 1.5$ mm, and $w_{\mathrm{wg}} = 4.8$ mm.

The dependencies of α/k_0 and β_{l} on these parameters are obtained through curve-fitting of simulation data. More specifically, in this analysis, the parameters are assumed to be independent. This allows us to write α/k_0 and β_{l} as a sum of four terms

$$\alpha/k_0 = c_1 + c_2 \cdot \kappa(ph_{\mathrm{l}}) + c_3 \cdot \nu(p_{\mathrm{l}}) + c_4 \cdot \tau(w_{\mathrm{wg}}) \quad (6)$$

$$\beta_{\mathrm{l}} = c_5 + c_6 \cdot \gamma(ph_{\mathrm{l}}) + c_7 \cdot \chi(p_{\mathrm{l}}) + c_8 \cdot \psi(w_{\mathrm{wg}}) \quad (7)$$

where $\kappa(\cdot)$, $\nu(\cdot)$, $\tau(\cdot)$, $\gamma(\cdot)$, $\chi(\cdot)$, and $\psi(\cdot)$ are curve-fit with a suitable function and $c_1 - c_8$ are obtained through multivariate linear regression. More details can be found in [46]. The correct aperture illumination is obtained by mapping the desired α/k_0- and β-profiles to the corresponding waveguide parameters through the fit curves. The α/k_0- and β-profiles are presented in Figs. 7(a) and 8(a) for the asymmetric and symmetric designs. The corresponding waveguide dimensions are presented in Figs. 7(b) and 8(b) for the asymmetric and symmetric designs. The mapping is only done for one frequency (60 GHz). The dimensions are indicated in Fig. 6(a) (inset).

B. Metasurface Prism

In Section II-B, the requirements on the refractive index inside the prism were outlined. Ideally, it should follow that of the effective refractive index of the leaky mode, which is rapidly increasing close to the cutoff of the guiding structure and then converges to 1 at high frequencies. However, such prisms are difficult to conceive in reality and we will therefore, in this article, limit the targeted bandwidth in which a reduced beam-squint is obtained. Moreover, we will allow for a small variation of the direction of maximum radiation ($\pm 0.5°$) after the waves are coupled through the prism. Taking these last two considerations into account, the constraints on the prism's refractive index are alleviated since the only requirement is to have a proper derivative of the refractive index with respect to frequency, in some frequency range.

An index-profile consistent with the above requirements is readily achieved using a metasurface. Moreover, since metasurfaces can be made fully metallic, they are attractive for high-frequency applications such as the one considered. In this article, the metasurface is implemented in a parallel plate bed-of-nails structure. Again, a holey metasurface could be used for increased robustness and decreased cost. However, due to the small air gap needed in the holey structure, which both

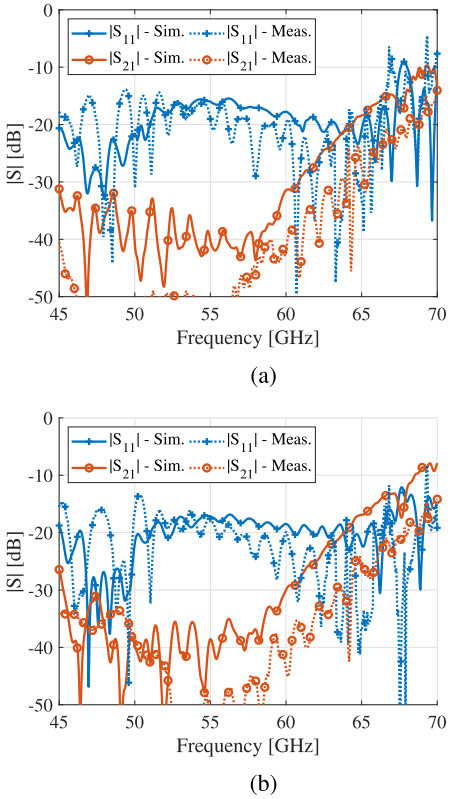

Fig. 9. S-parameters for the two designs. (a) Asymmetric. (b) Symmetric. The dimensions used for the simulations are given in Figs. 6–8. Additionally, the length of the leaky waveguide is $L_A = 100$ mm and the prism inclination is $\delta_p = 45°$, in both designs.

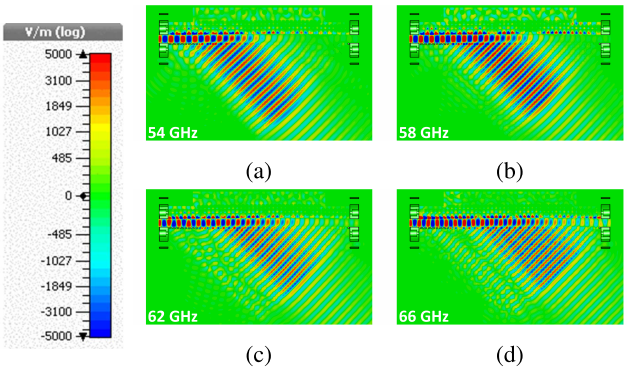

Fig. 10. Simulated electric field distribution (log-scale) for the asymmetric design. (a) 54 GHz, (b) 58 GHz, (c) 62 GHz, and (d) 66 GHz.

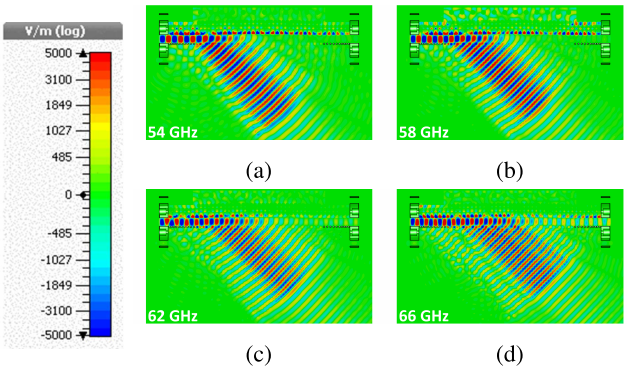

Fig. 11. Simulated electric field distribution (log-scale) for the symmetric design. (a) 54 GHz, (b) 58 GHz, (c) 62 GHz, and (d) 66 GHz.

requires accurate manufacturing and sophisticated impedance matching (to match to free-space), the bed-of-nails structure is preferred here.

The unit cell of the prism is depicted in Fig. 6(a) (in blue), together with the dispersion diagram (blue curve). The dimensions for the simulation are: $h_{wg} = 2.39$ mm, $ph_p = 0.7$ mm, $pw_p = 0.7$ mm, and $p_p = 1.3$ mm. From the dispersion curve, the effective refractive index of the prism is calculated as $n_{eff,prism} = \beta_p/k_0$, where β_p and k_0 are the propagation constants in the prism and in free-space, respectively. The effective refractive index of the leaky waveguide (for one sample along the waveguide) and the prism is presented in Fig. 6(b). For a range of frequencies (indicated with green in the figure), the ratio between the two indices remains approximately constant. Using (5), the final direction of maximum radiation (calculated based on infinite structures) is found, as illustrated in Fig. 6(c). A stable radiation, allowing $\pm 0.5°$ squinting, is obtained in the range 54–64 GHz and hence, roughly 20% bandwidth is achieved.

IV. Antenna Performance

The two designs are simulated in a full-wave solver. The asymmetric structure is only excited from one end of the leaky waveguide, while the symmetric structure is excited from both ends, sequentially (although simultaneous excitation is possible for a dual-beam radiation pattern). The waves travel along the leaky waveguide, slowly leaking their energy into the prism. The remaining energy at the far side of the waveguiding structure ($P_{diss} = P_{in}|S_{21}|^2$) is dissipated in a matched load. The length of the leaky waveguides is $L_A = 100$ mm ($= 20\lambda$) and the prism inclination is, in both designs, $\delta_p = 45°$. The remaining dimensions are as defined in the unit cell simulations and are given in Figs. 6–8.

The S-parameters are presented in Fig. 9(a) and (b) for the asymmetric and symmetric structures. For clarity, only the response from one port is shown in the symmetric design. The other port behaves the same due to the symmetry. A good matching is obtained throughout the band, with an $|S_{11}|$ below -15 dB in both designs. The periodic ripples in the $|S_{11}|$ are attributed to the presence of internal reflections in the antennas. The periodicity of the ripples, p_{ripple}, gives the distance from the excitation to the location at which the reflection occurs

$$d_{refl} = \frac{c}{2p_{ripple}} \tag{8}$$

where c is the speed of light. In our case, d_{refl} corresponds to the interface between the prism and free-space. The power transfer between the two ends of the waveguide, i.e., $|S_{21}|$, is below -15 dB ($\approx$3% power dissipated in the second port) throughout the band in both designs. Such a low value is usually not desired in LWAs since it might result in inefficiently used aperture (i.e., too fast leakage). However, since a leakage tapering is performed, the aperture is well illuminated in both designs, as illustrated with the x-component of the electric field in Figs. 10 and 11. Additionally, a low $|S_{21}|$ results

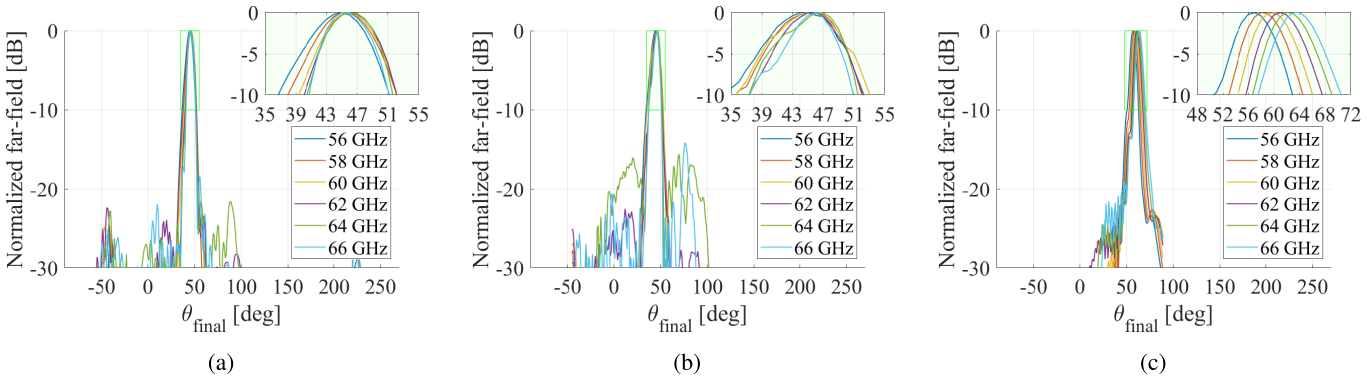

Fig. 12. Normalized H-plane radiation pattern for the asymmetric design. (a) Simulations, (b) measurements, and (c) case without prism (simulations).

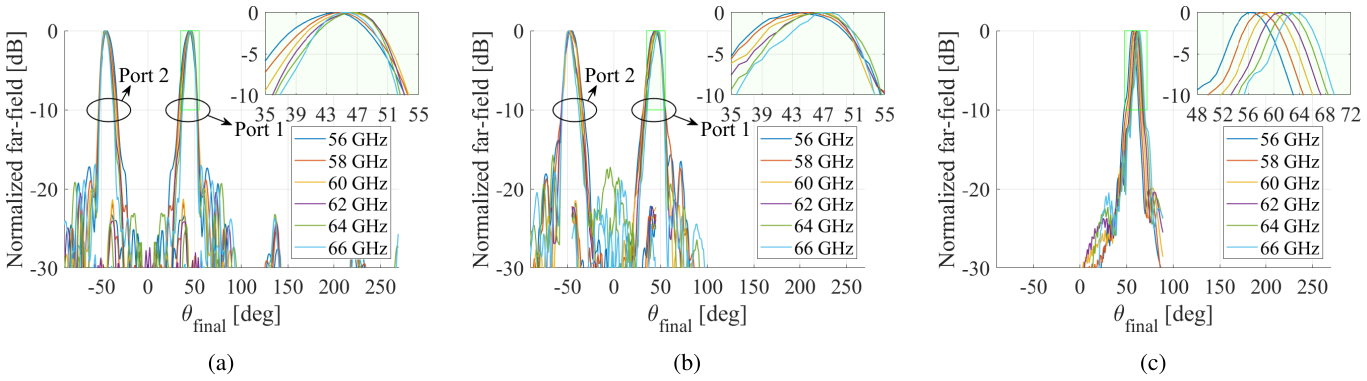

Fig. 13. Normalized H-plane radiation pattern for the symmetric design. (a) Simulations, (b) measurements, and (c) case without prism (simulations). The far-fields corresponding to ports 1 and 2 are overlapped in the same plot in postprocessing.

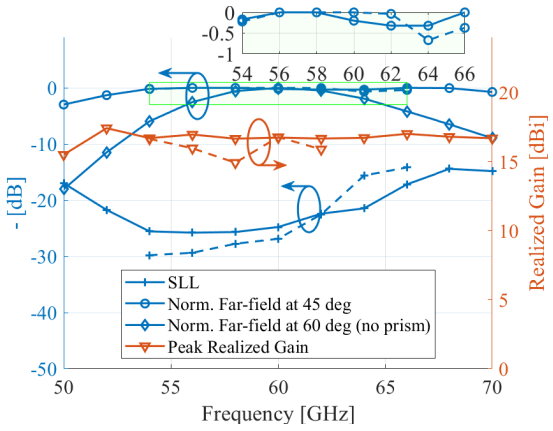

Fig. 14. Far-field characteristics for the asymmetric design. Simulations are plotted with solid lines and measurements are plotted with dashed lines.

in higher radiation efficiency, as the power is not dissipated in the load at the second port. In the measurements of the S-parameters, the effect of the transitions from waveguide to coaxial cable has been calibrated away since they introduced significant reflections in the upper part of the frequency band. The discrepancies between measurements and simulations in the $|S_{21}|$ are attributed to increased metallic losses due to the surface roughness (not included in simulations).

The normalized H-plane far-fields are presented in Figs. 12 and 13 for the asymmetric and symmetric designs, respectively. By comparing the results in Fig. 12(a) with Fig. 12(c) and Fig. 13(a) with Fig. 13(c), which corresponds to the simulated cases of a leaky waveguide with and without prism, for the asymmetric and symmetric designs, respectively, it is clear that the beam-squint is significantly reduced by coupling the radiation through a prism. The measurements of the far-field, presented in Figs. 12(b) and 13(b) for the two designs, corroborates the simulations. The radiation pattern at a specific direction, normalized to the peak value, is presented in Figs. 14 and 15, for the two designs, together with the realized gain and sidelobe level. Again, it is clear that by coupling the radiation through a prism, decreased beam-squint is obtained. At 45°, a maximum of 0.5 and 1 dB scan-loss is obtained in the asymmetric and symmetric designs, respectively. Moreover, the realized gain is stable at roughly 17 and 15 dBi for the two designs throughout the band. The observed ripples in the S-parameters are small and they have no noticeable effect on the gain. Sidelobes below -20 and -17 dB are obtained in the asymmetric and symmetric designs, respectively. In the asymmetric design, the measured sidelobes are higher than the simulated in the upper part of the operating band. A similar increase in the sidelobes is observed in simulations for higher frequencies (66–70 GHz). Due to the high reflections from the transitions at the higher frequencies, the gain is not measured at frequencies above 62 GHz. A small drop in the measured gain is observed at 58 GHz. Other than that, the measurements agree well with simulations in all the far-field characteristics. The obtained total efficiency for the two antennas.

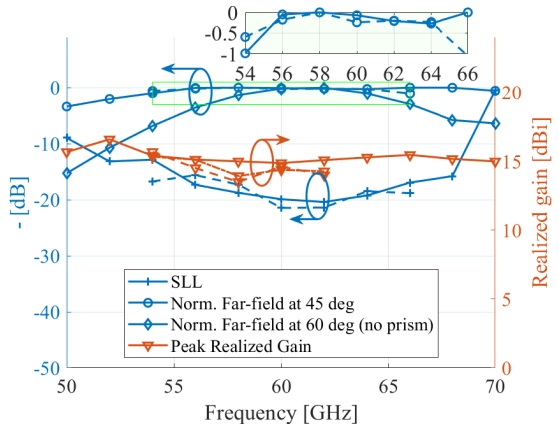

Fig. 15. Far-field characteristics for the symmetric design. Simulations are plotted with solid lines and measurements are plotted with dashed lines.

TABLE I
SIMULATED TOTAL EFFICIENCY OF THE TWO ANTENNAS

Frequency [GHz]:	54	58	62	66
Asymmetric:	88%	89%	87%	85%
Symmetric:	90%	90%	89%	85%

(in simulation) is presented in Table I. Almost 90% efficiency is achieved throughout the band.

V. CONCLUSION

In this article, two novel nondispersive LWAs are presented, operating at 60 GHz. The antennas utilize a dispersive lens to cancel the dispersion of the feeding leaky waveguide, thus, obtaining a nonsquinting radiation pattern with respect to frequency. Unlike previous works, a leakage tapering is performed along the aperture which results in reduced sidelobe levels. One asymmetrically and one symmetrically tapered antenna is designed and manufactured. The asymmetric antenna is optimized for the lowest possible sidelobes with a single-beam operation and the symmetric antenna is optimized for the lowest possible sidelobes, under the constraint of symmetric tapering with respect to broadside. The symmetry in the latter design results in slightly increased sidelobes, compared to the asymmetric design, but enables two beams that can be obtained either independently or jointly. To the best of our knowledge, this is the first multibeam low-dispersive LWA reported in the literature. High efficiency and low losses are achieved at 60 GHz by implementing the antennas in groove gap waveguide technology. Both antennas achieve a beam squint smaller than 1° over a 20% bandwidth and the total efficiency is almost 90% throughout the band in both designs. A stable gain of 17 and 15 dBi is achieved in the asymmetric and symmetric designs, respectively. The antennas are manufactured and measurements corroborate simulations. No LWA with similar or better performance in terms of radiation pattern stability, SLL, bandwidth, and efficiency (90%) has been reported in the literature, especially considering the high operating frequency. The antennas are intended for mmWave point-to-point links in future communication systems (5G and beyond).

ACKNOWLEDGMENT

The authors would like to thank A. Alex-Amor and Á. Palomares-Caballero for their help during the far-field measurement of the prototypes.

REFERENCES

[1] A. U. Zaman and P. Kildal, "Gap waveguides," in *Handbook of Antenna Technologies*. Singapore: Springer, 2016.
[2] E. Rajo-Iglesias, M. Ferrando-Rocher, and A. U. Zaman, "Gap waveguide technology for millimeter-wave antenna systems," *IEEE Commun. Mag.*, vol. 56, no. 7, pp. 14–20, Jul. 2018.
[3] A. U. Zaman, P.-S. Kildal, and A. A. Kishk, "Narrow-band microwave filter using high-Q groove gap waveguide resonators with manufacturing flexibility and no sidewalls," *IEEE Trans. Compon., Packag., Manuf. Technol.*, vol. 2, no. 11, pp. 1882–1889, Nov. 2012.
[4] E. Pucci, A. U. Zaman, E. Rajo-Iglesias, P.-S. Kildal, and A. Kishk, "Study of Q-factors of ridge and groove gap waveguide resonators," *IET Microw., Antennas Propag.*, vol. 7, no. 11, pp. 900–908, Aug. 2013.
[5] E. Rajo-Iglesias, M. Ebrahimpouri, and O. Quevedo-Teruel, "Wideband phase shifter in groove gap waveguide technology implemented with glide-symmetric holey EBG," *IEEE Microw. Wireless Compon. Lett.*, vol. 28, no. 6, pp. 476–478, Jun. 2018.
[6] A. Vosoogh and P.-S. Kildal, "Corporate-fed planar 60-GHz slot array made of three unconnected metal layers using AMC pin surface for the gap waveguide," *IEEE Antenna Wireless Propag. Lett.*, vol. 15, pp. 1935–1938, 2015.
[7] D. Zarifi, A. Farahbakhsh, A. U. Zaman, and P. S. Kildal, "Design and fabrication of a high-gain 60-GHz corrugated slot antenna array with ridge gap waveguide distribution layer," *IEEE Trans. Antennas Propag.*, vol. 64, no. 7, pp. 2905–2913, Jul. 2016.
[8] M. A. Sharkawy, A. Foroozesh, A. A. Kishk, and R. Paknys, "A robust horn ridge gap waveguide launcher for metal strip grating leaky wave antenna," *IEEE Trans. Antennas Propag.*, vol. 62, no. 12, pp. 6019–6026, Dec. 2014.
[9] M. Vukomanovic, J.-L. Vazquez-Roy, O. Quevedo-Teruel, E. Rajo-Iglesias, and Z. Sipus, "Gap waveguide leaky-wave antenna," *IEEE Trans. Antennas Propag.*, vol. 64, no. 5, pp. 2055–2060, May 2016.
[10] H. Wang, R. Gao, Y. Gu, J. Cao, and Z. Ye, "Low sidelobe leaky wave antenna based on gap waveguide technology," in *Proc. Int. Appl. Comput. Electromagn. Soc. Symp. (ACES)*, Aug. 2017, pp. 1–2.
[11] D. R. Jackson and A. A. Oliner, "Leaky-wave antennas," in *Modern Antenna Handbook*. Hoboken, NJ, USA: Wiley, 2007, pp. 325–367.
[12] W. Hong, T.-L. Chen, C.-Y. Chang, J. W. Sheen, and Y.-D. Lin, "Broadband tapered microstrip leaky-wave antenna," *IEEE Trans. Antennas Propag.*, vol. 51, no. 8, pp. 1922–1928, Aug. 2003.
[13] N. Nguyen-Trong, T. Kaufmann, and C. Fumeaux, "A semi-analytical solution of a tapered half-mode substrate-integrated waveguide with application to rapid antenna optimization," *IEEE Trans. Antennas Propag.*, vol. 62, no. 6, pp. 3189–3200, Jun. 2014.
[14] N. Nguyen-Trong, L. Hall, T. Kaufmann, and C. Fumeaux, "Wideband millimeter-wave antennas with magnetic-dipole patterns integrated in metallic structures," *IEEE Trans. Antennas Propag.*, vol. 64, no. 11, pp. 4877–4882, Nov. 2016.
[15] A. Neto, S. Bruni, G. Gerini, and M. Sabbadini, "The leaky lens: A broad-band fixed-beam leaky-wave antenna," *IEEE Trans. Antennas Propag.*, vol. 53, no. 10, pp. 3240–3246, Oct. 2005.
[16] J. L. Gómez-Tornero, A. Martínez-Ros, A. Álvarez-Melcón, F. Mesa, and F. Medina, "Substrate integrated waveguide leaky-wave antenna with reduced beam squint," in *Proc. Eur. Microw. Conf. (EuMC)*, Dec. 2013, pp. 491–494.
[17] J. L. Gómez-Tornero, M. Poveda-García, R. Guzmán-Quirós, and D. Cañete-Rebenaque, "Reducing the beam squint in scanned leaky-wave antennas using coupled SIW cavities," *Antennas Propag. Soc. Int. Symp. (APS/URSI)*, Oct. 2016, pp. 77–78.
[18] H. Mirzaei and G. V. Eleftheriades, "Arbitrary-angle squint-free beamforming in series-fed antenna arrays using non-foster elements synthesized by negative-group-delay networks," *IEEE Trans. Antennas Propag.*, vol. 63, no. 5, pp. 1997–2010, May 2015.
[19] A. Porokhnyuk, T. Ueda, Y. Kado, and T. Itoh, "Nonreciprocal metamaterial for non-squinting leaky-wave antenna with enhanced beam steering," in *Proc. IEEE Antennas Propag. Soc. Int. Symp. (APSURSI)*, Jul. 2013, pp. 2289–2290.

[20] K. M. Kossifos and M. A. Antoniades, "A NRI-TL metamaterial leaky-wave antenna radiating at broadside with zero beam-squinting," *IEEE Antennas Wireless Propag. Lett.*, vol. 17, no. 12, pp. 2223–2227, Dec. 2018.

[21] A. Mehdipour, J. W. Wong, and G. V. Eleftheriades, "Beam-squinting reduction of leaky-wave antennas using huygens metasurfaces," *IEEE Trans. Antennas Propag.*, vol. 63, no. 3, pp. 978–992, Mar. 2015.

[22] L. Wang, J. L. Gómez-Tornero, and O. Quevedo-Teruel, "Substrate integrated waveguide leaky-wave antenna with wide bandwidth via prism coupling," *IEEE Trans. Microw. Theory Techn.*, vol. 66, no. 6, pp. 3110–3118, Jun. 2018.

[23] L. Wang, J. L. Gómez-Tornero, E. Rajo-Iglesias, and O. Quevedo-Teruel, "Low-dispersive leaky-wave antenna integrated in groove gap waveguide technology," *IEEE Trans. Antennas Propag.*, vol. 66, no. 11, pp. 5727–5736, Nov. 2018.

[24] O. Quevedo-Teruel, M. Ebrahimpouri, and F. Ghasemifard, "Lens antennas for 5G communications systems," *IEEE Commun. Mag.*, vol. 56, no. 7, pp. 36–41, Jul. 2018.

[25] J. L. Gómez-Tornero, A. J. Martínez-Ros, and R. Verdú-Monedero, "FFT synthesis of radiation patterns with wide nulls using tapered leaky-wave antennas," *IEEE Antennas Wireless Propag. Lett.*, vol. 9, pp. 518–521, 2010.

[26] A. A. Oliner, "Leaky-wave antennas," in *Antenna Engineering Handbook*. New York, NY, USA: McGraw-Hill, 1993, pp. 262–321.

[27] A. J. Martinez-Ros, J. L. Gómez-Tornero, and G. Goussetis, "Holographic pattern synthesis with modulated substrate integrated waveguide line-source leaky-wave antennas," *IEEE Trans. Antennas Propag.*, vol. 61, no. 7, pp. 3466–3474, Jul. 2013.

[28] J. L. Gómez-Tornero, A. T. Martinez, D. C. Rebenaque, M. Gugliemi, and A. Álvarez-Melcón, "Design of tapered leaky-wave antennas in hybrid waveguide-planar technology for millimeter waveband applications," *IEEE Trans. Antennas Propag.*, vol. 53, no. 8, pp. 2563–2577, Aug. 2005.

[29] P.-S. Kildal, E. Alfonso, A. Valero-Nogueira, and E. Rajo-Iglesias, "Local metamaterial-based waveguides in gaps between parallel metal plates," *IEEE Antennas Wireless Propag. Lett.*, vol. 8, pp. 84–87, 2008.

[30] E. Rajo-Iglesias and P.-S. Kildal, "Groove gap waveguide: A rectangular waveguide between contactless metal plates enabled by parallel-plate cut-off," in *Proc. 4th Eur. Conf. Antennas Propag.*, Apr. 2010, pp. 1–4.

[31] E. Pucci, "Gap waveguide technology for millimeter wave applications and integration with antennas," Ph.D. dissertation, Dept. Signals Syst., Chalmers Univ. Technol., Gothenburg, Sweden, Nov. 2013.

[32] M. Ebrahimpouri, O. Quevedo-Teruel, and E. Rajo-Iglesias, "Design guidelines for gap waveguide technology based on glide-symmetric holey structures," *IEEE Microw. Wireless Compon. Lett.*, vol. 27, no. 6, pp. 542–544, Jun. 2017.

[33] M. Ebrahimpouri, E. Rajo-Iglesias, Z. Sipus, and O. Quevedo-Teruel, "Cost-effective gap waveguide technology based on glide-symmetric holey EBG structures," *IEEE Trans. Microw. Theory Techn.*, vol. 66, no. 2, pp. 927–934, Feb. 2018.

[34] A. Hessel, M. H. Chen, R. C. M. Li, and A. A. Oliner, "Propagation in periodically loaded waveguides with higher symmetries," *Proc. IEEE*, vol. 61, no. 2, pp. 183–195, Feb. 1973.

[35] O. Quevedo-Teruel, M. Ebrahimpouri, and M. N. M. Kehn, "Ultrawideband metasurface lenses based on off-shifted opposite layers," *IEEE Antennas Wireless Propag. Lett.*, vol. 15, pp. 484–487, 2016.

[36] O. Quevedo-Teruel, J. Miao, M. Mattsson, A. Algaba-Brazalez, M. Johansson, and L. Manholm, "Glide-symmetric fully metallic luneburg lens for 5G communications at ka-band," *IEEE Antennas Wireless Propag. Lett.*, vol. 17, no. 9, pp. 1588–1592, Sep. 2018.

[37] D. Cavallo and C. Felita, "Analytical formulas for artificial dielectrics with nonaligned layers," *IEEE Trans. Antennas Propag.*, vol. 65, no. 10, pp. 5303–5311, Oct. 2017.

[38] D. Cavallo, "Dissipation losses in artificial dielectric layers," *IEEE Trans. Antennas Propag.*, vol. 66, no. 12, pp. 7460–7465, Dec. 2018.

[39] T. Chang *et al.*, "Broadband giant-refractive-index material based on mesoscopic space-filling curves," *Nature Commun.*, vol. 7, Aug. 2016, Art. no. 12661.

[40] F. Ghasemifard, M. Norgren, O. Quevedo-Teruel, and G. Valerio, "Analyzing glide-symmetric holey metasurfaces using a generalized floquet theorem," *IEEE Access*, vol. 6, pp. 71743–71750, 2018.

[41] F. Ghasemifard, M. Norgren, and O. Quevedo-Teruel, "Dispersion analysis of 2-D glide-symmetric corrugated metasurfaces using mode-matching technique," *IEEE Microw. Wireless Compon. Lett.*, vol. 28, no. 1, pp. 1–3, Jan. 2018.

[42] G. Valerio, F. Ghasemifard, Z. Sipus, and O. Quevedo-Teruel, "Glide-symmetric all-metal holey metasurfaces for low-dispersive artificial materials: Modeling and properties," *IEEE Trans. Microw. Theory Techn.*, vol. 66, no. 7, pp. 3210–3223, Jul. 2018.

[43] Q. Chen, F. Ghasemifard, G. Valerio, and O. Quevedo-Teruel, "Modeling and dispersion analysis of coaxial lines with higher symmetries," *IEEE Trans. Microw. Theory Techn.*, vol. 66, no. 10, pp. 4338–4345, Oct. 2018.

[44] A. Vosoogh, Z. S. He, and H. Zirath, "A cost-effective D-band multilayer rectangular waveguide transmission line based on glide-symmetric EBG structure," in *Proc. 12th Eur. Conf. Antennas Propag. (EuCAP)*, Dec. 2018, pp. 1–4.

[45] M. Ebrahimpouri, A. A. Brazalez, L. Manholm, and O. Quevedo-Teruel, "Using glide-symmetric holes to reduce leakage between waveguide flanges," *IEEE Microw. Wireless Compon. Lett.*, vol. 28, no. 6, pp. 473–475, Jun. 2018.

[46] O. Dahlberg, "Low-dispersive leaky-wave antennas: A viable approach for fifth generation (5G) mmWave base station antennas," M.S. thesis, Division Electromagn. Eng., KTH Roy. Inst. Technol., Stockholm, Sweden, Jun. 2019.

Oskar Zetterstrom (S'17) received the B.Sc. and M.Sc. degrees in electrical engineering and electromagnetic engineering from the KTH Royal Institute of Technology, Stockholm, Sweden, in 2016 and 2019, respectively, where he is currently pursuing the Ph.D. degree, with a focus on electromagnetics and antennas.

In 2019, he joined the Department of Electromagnetic Engineering, KTH Royal Institute of Technology. He has authored and coauthored over several journal and conference articles. His current research interests include transformation optics, lens antennas, metamaterials possessing higher symmetries, and leaky-wave antennas.

Mr. Zetterstrom has been awarded the first price in the Student Design Competition at APS/URSI 2016 in Puerto Rico and the IEEE Eugene F. Knott Research Grant for his works.

Elena Pucci received the M.Sc. degree in telecommunication engineering from the University of Siena, Italy, in 2008 and the Ph.D. degree from the Chalmers University of Technology, Gothenburg, Sweden, in 2013.

She joined Ericsson AB, Stockholm, Sweden, in 2014, where she is currently a Researcher in antenna technologies for 5G. She has authored and coauthored several publications in journals and conferences. Her current research interests include antenna design for millimeter wave applications, antenna arrays, metasurfaces, and OTA testing.

Dr. Pucci was a recipient of the Second-Best Student Paper Award at the European Conference on Antennas and Propagation (EuCAP 2012) in 2012 and the Best Poster Award at Micromechanics and Microsystems Europe Workshop in 2012.

Pablo Padilla was born in Jaén, Spain, in 1982. He received the degree in telecommunication engineering and the Ph.D. degree from the Radiation Group of the Signal, Systems and Radio communications Department, Technical University of Madrid (UPM), Madrid, Spain, in 2005 and 2009, respectively.

In 2007, he was with the Laboratory of Electromagnetics and Acoustics, École Polytechnique Fédérale de Lausanne, Lausanne, Switzerland, as an invited Ph.D. Student. In 2009, he carried out a postdoctoral stay at the Helsinki University of Technology (AALTO-TKK), Espoo, Finland. In 2009, he became an Assistant Professor with the Signal Theory, Telematics and Communications Department, University of Granada, Granada, Spain, where he has been an Associate Professor since 2012. In 2017, he was a Visiting Professor with the Royal Institute of Technology of Stockholm, Stockholm Sweden. He has authored over 60 high-impact journal contributions and more than 50 contributions to international symposia. His current research interests include a variety area of knowledge related mainly to electromagnetism and communication topics (radio frequency devices, antennas, and propagation).

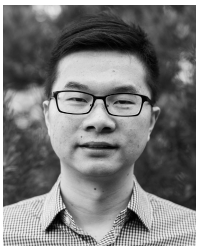

Lei Wang (S'09–M'15–SM'19) received the Ph.D. degree in electromagnetic field and microwave technology from Southeast University, Nanjing, China, in 2015.

From September 2014 to September 2016, he was a Research Fellow and Post-Doctoral Researcher with the Laboratory of Electromagnetics and Antennas (LEMA), Swiss Federal Institute of Technology (EPFL), Lausanne, Switzerland. From October 2016 to November 2017, he was a Post-Doctoral Research Fellow with the Electromagnetic Engineering Laboratory, KTH Royal Institute of Technology, Stockholm, Sweden. Since 2017, he has been an Alexander von Humboldt Fellow with the Institute of Electromagnetic Theory, Hamburg University of Technology (TUHH), Hamburg, Germany. His current research interests include the antenna theory and applications, active electronically scanning arrays (AESAs), integrated antennas and arrays, substrate-integrated waveguide antennas, leaky-wave antennas, and wireless propagation.

Dr. Wang was awarded the Chinese National Scholarship for Ph.D. Candidates in 2014 and was granted the Swiss Government Excellence Scholarship to conduct research on SIW horn antennas and applications in 2014. He was also granted by the Alexander von Humboldt Research Foundation to take research on antenna modeling and optimization in 2016. He was a recipient of the Best Poster Award in 2018 IEEE International Workshop on Antenna Technology (iWAT).

Oscar Quevedo-Teruel (M'10–SM'17) received the degree in telecommunication engineering from the Carlos III University of Madrid, Madrid, Spain, in 2005, part of which was done at Chalmers University of Technology, Gothenburg, Sweden, and the Ph.D. degree from the Carlos III University of Madrid, in 2010.

He was invited as a Post-Doctoral Researcher with the University of Delft, Delft, The Netherlands. From 2010 to 2011, he was a Research Fellow with the Department of Theoretical Physics of Condensed Matter, Universidad Autonoma de Madrid, Madrid. He was a Post-Doctoral Researcher with the Queen Mary University of London, London, U.K., from 2011 to 2013. In 2014, he joined the Electromagnetic Engineering Division, School of Electrical Engineering and Computer Science, KTH Royal Institute of Technology in Stockholm, Stockholm, Sweden, where he is currently an Associate Professor and the Director of the Master Program in Electromagnetics Fusion and Space Engineering. He has authored and coauthored over 77 articles in international journals, 130 at international conferences. He has received approval for four patents.

Dr. Quevedo-Teruel has been an Associate Editor of the IEEE TRANSACTIONS ON ANTENNAS AND PROPAGATION since 2018. He is a Distinguished Lecturer of the IEEE Antennas and Propagation Society from 2019 to 2021. He is the delegate of EurAAP for Sweden, Norway, and Iceland from 2018 to 2020.